Short Communication

Causes of Germanium Phosphide Degradation under Prolonged Cycling. EIS Study

Tatiana Kulova[1], Dmitrii Gryzlov[1], Alexander Skundin[1], Ilya Gavrilin[1,2], Irina Martynova[2], Yulia Kudryashova[1]

[1] Frumkin Institute of Physical Chemistry and Electrochemistry of the Russian Academy of Sciences, 31-4 Leninskii ave., 119071 Moscow, Russia
[2] National Research University of Electronic Technology (MIET), Bld. 1, Shokin Square, Zelenograd, 124498, Moscow, Russia
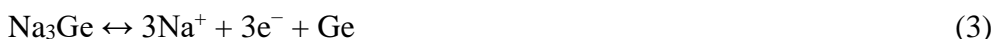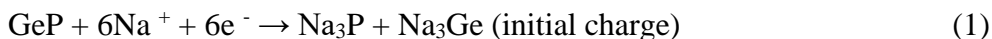[*]E-mail: askundin@mail.ru

Negative electrodes (anodes) of a germanium-phosphide-based sodium-ion battery were cycled at different current densities. Germanium phosphide impedance spectra were measured and analyzed for different cycles. It was found that prolonged cycling at low current densities (0.02 C) leads to an increase in the resistance of the solid electrolyte film and the consequent increase in the effective charge transfer resistance. It was concluded that changes in these equivalent circuit parameters cause the degradation of germanium phosphide under cycling.

1. INTRODUCTION

Germanium phosphide (GeP) is regarded as a promising, albeit poorly studied, negative electrode (anode) material for sodium-ion batteries [1−5]. This material is produced by high-energy ball-milling [3, 4], solid-phase synthesis [5], or solvothermal synthesis [1]. In all the papers mentioned, GeP-based electrodes have sufficient specific capacity, but the results obtained in different papers vary a lot. In addition, it is reported that all electrodes show degradation (capacity reduction) during cycling, but the rate of degradation in different papers also varies. The mechanism of reversible sodium insertion into GeP-based materials is still a matter of debate. In [6] based on experimental data [2], it is declared that initial sodium ion insertion takes place between GeP layers to form Na_xGeP ($0<x<1/3$), after which the alloys of Na_yGe and Na_zP are formed, where ($0 <y \leq 3.75$) and ($0 <z \leq 3$). At the maximum sodiation

degree, the mechanism of reversible sodium insertion into GeP can be described by the following equations (1−3):

$$GeP + 6Na^+ + 6e^- \rightarrow Na_3P + Na_3Ge \text{ (initial charge)} \qquad (1)$$

$$Na_3P \leftrightarrow 3Na + 3e^- + P \qquad (2)$$

$$Na_3Ge \leftrightarrow 3Na^+ + 3e^- + Ge \qquad (3)$$

In this case, the theoretical GeP capacity, calculated according to Faraday's laws, will be about 1550 mAh/g.

Our previous work [7] described electrodes obtained by red phosphorus evaporation-condensation on germanium nanowires electrodeposited from an aqueous electrolyte on a titanium substrate. These electrodes had a reversible sodium insertion capacity of about 1300 mAh/g at a rate of 0.019 C and about 130 mAh/g at 0.3 C. In the present work, we apply the method of electrochemical impedance spectroscopy to investigate the degradation mechanism of such electrodes during long-term cycling.

Electrochemical impedance spectroscopy is widely used to analyze the degradation of both lithium-ion and sodium-ion batteries [8–10] and individual electrodes of these batteries during cycling [11–15]. At the same time, the results of studies of germanium phosphide electrodes by electrochemical impedance spectroscopy are not available in the literature.

2. EXPERIMENTAL

2.1. GeP synthesis

The GeP synthesis is described in detail in [7]. Initially, germanium nanowires were synthesized on titanium foil substrates. The nanowires deposition technique is described in detail in [16, 17]. A visual schematic representation of the GeP synthesis is shown in Fig. 1.
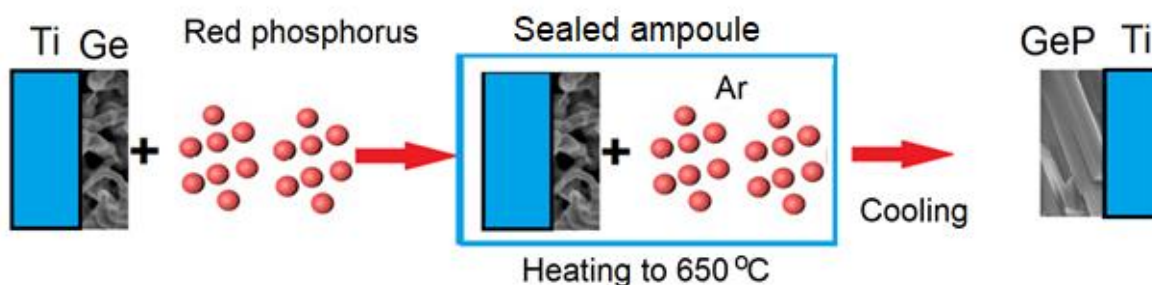

Figure 1. Schematic representation of GeP synthesis.

Preparation of phosphorus for synthesis was carried out as follows: phosphorus powder was soaked in ethanol for 4 hours, then excess ethanol was poured off and a container with wet phosphorus was placed in a desiccator with P_2O_5. The desiccator was purged with argon and left for a day to evaporate ethanol. Next, dry phosphorus powder was placed in a sealed glass container and dried under

Int. J. Electrochem. Sci., 17 **(2022)** Article Number: 220224

3

vacuum at 120 ° C to completely remove traces of water. Vacuum-dried phosphorus powder was placed in a glove box with an argon atmosphere.

2.2 Characterization of GeP

The synthesized samples of GeP were characterized by scanning electron microscopy (SEM) as well as by X-Ray diffraction (XRD). The corresponding instruments and techniques are described in detail in [7].

2.3 Electrochemical research

To characterize the electrodes, we carried out galvanostatic cycling and recorded electrochemical impedance spectra at different cycling stages. Detailed conditions for the assembly of electrochemical cells, the composition of the electrolyte, the type of equipment used and the conditions for electrochemical measurements are also described in [7].

The sodium insertion corresponds to charging in the sodium-ion battery; the reverse process corresponds to discharging the sodium-ion battery. For this reason, the capacity recorded at cathodic polarization was referred to as charge capacity, whereas the capacity recorded at anodic polarization was referred to as discharge capacity. The charge and discharge capacities were evaluated by galvanostatic cycling at different current densities.

3. RESULTS AND DISCUSSION

3.1. Morphological and physicochemical studies

Fig. 2 shows SEM images of the synthesized GeP sample. Fig. 2a shows a frontal image at various magnifications. Fig. 2b shows an image of the cross cleavage of the sample. It can be seen that GeP comes in the form of nanorods with diameters between 250 and 500 nm and lengths between 0.2 and 10 μm. The GeP layer thickness estimated from Fig. 2b was about 4 μm.
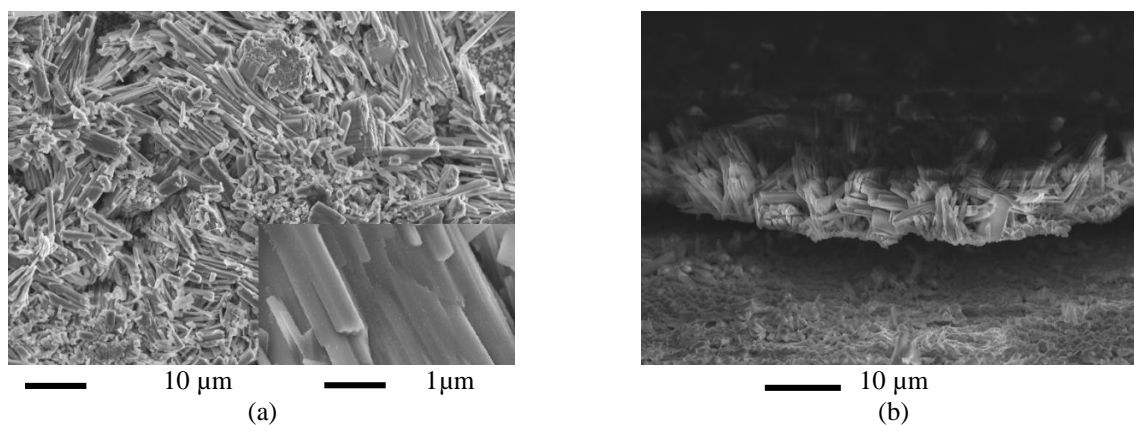

Figure 2. SEM images of a frontal surface (a) and cross cleavage (b) of GeP samples. The magnifications are shown on the figure.

The X-ray diffractogram of the synthesized GeP shown in Fig.3 points to GeP formation.
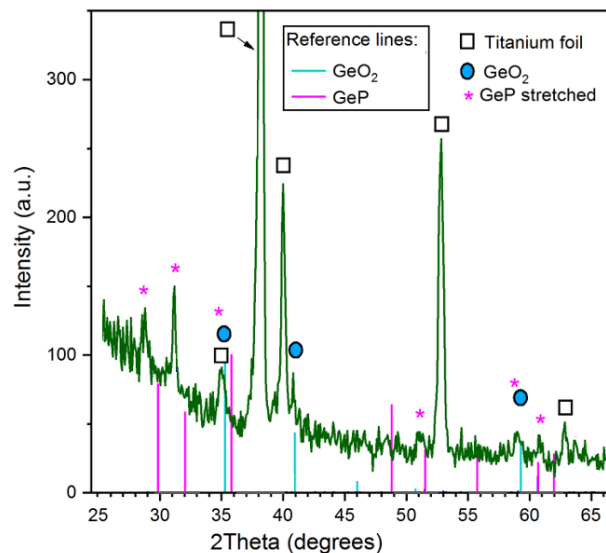

Figure 3. X-ray diffractogram of GeP sample on titanium substrate

A slight shift of the GeP-related peaks compared to COD (Crystallography Open Database) data suggests that the lattice of this phase is somewhat stretched. In the spectrum, there are also some peaks related to germanium oxide GeO_2.

3.2 Electrochemical measurements. GeP prolonged cycling.

The change in discharge capacity during cycling is shown in Fig. 4a. The same Figure shows the change in the Coulomb efficiency, i.e., the ratio of the anode capacity to the cathode one. The cycling efficiency for the first cycle can be seen to make up 65%, i.e., during the first cathodic polarization, a large proportion of the irreversible processes associated with solid electrolyte film (SEI) formation takes place on the electrode. For the subsequent charging-discharging cycles, the Coulomb efficiency gradually increases and remains constant from cycle 20 to cycle 100. Fig. 4b shows the charging and discharging curves of GeP for 1−8, 12, 40, and 90 cycles at a current density of 30 mA/g. The curves in Fig. 4 show that with a current density of 30 mA/g, corresponding to 0.017C, the discharge capacity was 1300 mAh/g (about 84% of the theoretical capacity when sodium is inserted in GeP). Analysis of Fig. 4a demonstrates that for GeP, the first eight charging-discharging cycles saw the sharpest drop in the discharge capacity, about 0.83% per cycle. From cycle 12 to 70, the degradation trend was about 0.46% per cycle, and from cycle 70 to 100 about 0.32% per cycle.
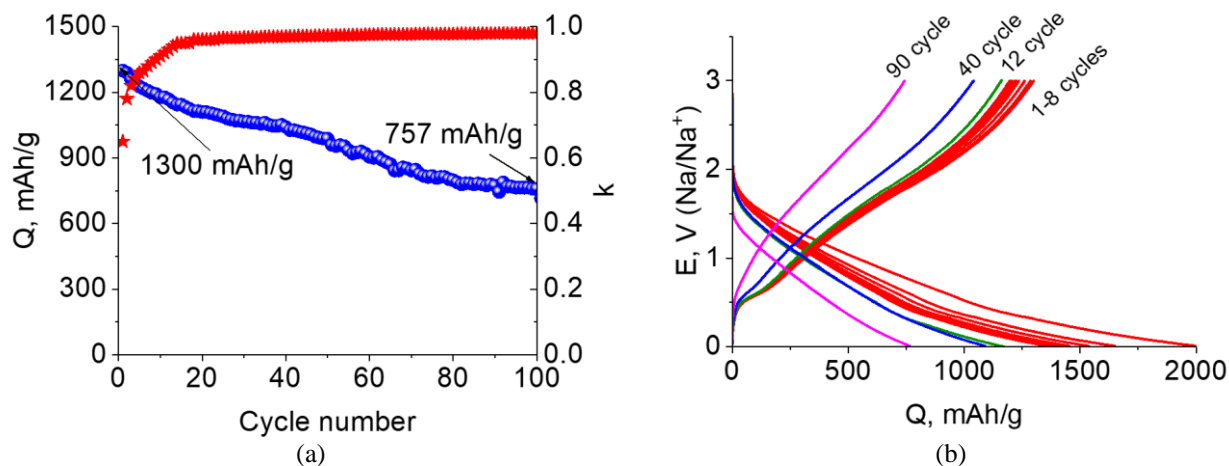
Figure 4. Change in discharge capacity Q and Coulomb efficiency k (a) and charging-discharging curves of GeP (b) in 1M $NaClO_4$ in propylene carbonate-ethylene carbonate (1:1). The current density is 30 mA /g.

As we mentioned in the Introduction, electrochemical impedance spectroscopy is a convenient tool for determining the causes of degradation of electrode materials under prolonged cycling. Fig. 5 shows the GeP impedance spectra recorded at the first, fortieth, seventieth, ninetieth, and hundredth cycles. To simulate the impedance spectra, we used the equivalent circuit shown in Fig. 5b. The equivalent circuit includes electrolyte resistance (R_s), SEI resistance (R_f), SEI capacitance (C_f), charge transfer resistance (R_{ct}), constant phase shift element (CPE) characterizing the capacitance of the electric double layer, and Warburg element (Wo) characterizing the solid phase diffusion of the sodium. The authors have previously used the same equivalent circuit to investigate the insertion of lithium and sodium into GeP [7] and the insertion of lithium into nanostructured germanium nanowires [17]. It should be noted that no data on impedance spectroscopy of GeP-based electrodes in reversible sodium insertion processes are available in the literature. Only a few papers present the results of studying germanium phosphides during the insertion/extraction of lithium, e.g., in [18], the impedance spectra of newly fabricated GeP and GeP/nitrogen-doped-carbon-composite electrodes are given, and it is concluded that the charge transfer resistance for GeP-carbon composite is lower than that of GeP. [19] gives impedance spectra of GP flakes electrodes after 100 cycles of lithium insertion/extraction under cycling in different cycling ranges. This latter paper uses the same equivalent circuit as the present paper and concludes that a wider cycling range (0.001−3 V instead of 0.001−0.85 V) leads to higher solid electrolyte film resistance and charge transfer resistance; however, no data on the dynamics of these parameters during cycling are available.
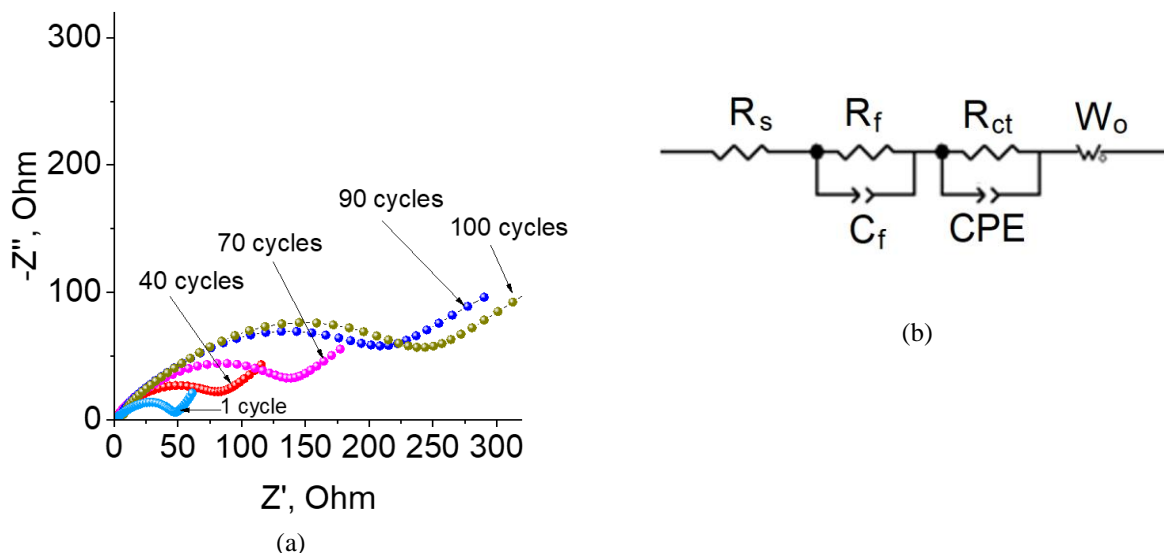
Figure 5. GeP impedance spectra recorded at different cycles (a) and the equivalent circuit for modeling impedance spectra (b).

As can be seen from Fig. 5, there is a significant increase in electrode impedance during cycling. Table 1 shows the equivalent circuit elements for the impedance spectra measured at the 1st, 40th, 70th, 90th, and 100th cycles.

Table 1. The equivalent circuit parameters at the 1st, 40th, 70th, 90th, and 100th cycles.

Cycle Number	R_s, Ohm	R_f, Ohm·cm^2	C_f, F / cm^2	R_{ct}, Ohm·cm^2	C_{dl}, F /cm^2	W_o, Ohm/s$^{1/2}$	D_{eff}, cm^2/s
1	1.4	16.0	$5.2 \cdot 10^{-6}$	205.0	$4.8 \cdot 10^{-6}$	30.6	$6.0 \cdot 10^{-14}$
40	1.7	20.5	$3.8 \cdot 10^{-6}$	288.0	$3.9 \cdot 10^{-6}$	122.6	$4.0 \cdot 10^{-15}$
70	2.3	38.5	$2.1 \cdot 10^{-6}$	544.0	$2.95 \cdot 10^{-6}$	184.2	$1.6 \cdot 10^{-15}$
90	2.6	65.5	$1.6 \cdot 10^{-6}$	732.5	$3.0 \cdot 10^{-6}$	248.0	$1.0 \; 10^{-15}$
100	2.6	67.0	$1.6 \cdot 10^{-6}$	735.0	$2.8 \cdot 10^{-6}$	259.3	$0.9 \cdot 10^{-15}$

The capacitance of the double layer at the interface (C_{dl}) was calculated using the equation:

$$C_{dl}=T^{1/P}R_{ct}^{(1/P-1)}, \tag{4}$$

where T is (CPE-T), and P is (CPE-P)

The values of the Warburg constant were determined by the equation:

$$W=W_R/(2*W_T)^{Wp} \tag{5}.$$

Analysis of Table 1 shows a regular change in the numerical values of the equivalent circuit parameters during cycling. Here D_{eff} is sodium ion effective diffusion coefficient. The parameters R_s, R_f, $1/C_f$, R_{ct} and $1 / D_{eff}$ increase and their dependences on cycle numbers are close to linear. The quantitative rise in all these parameters is undoubtedly due to a gradual increase in SEI and a change in its porosity. Indeed, the SEI formation at germanium, alike as at silicon and tin (but unlike to carbon) is known to continue for whole cycling period (see, e.g. [20−22]). The SEI average thickness continuously increases

whereas its porosity slightly decreases. These phenomena are reflected by almost synchronous decrease in Cf and increase in Rf. Significant share of Rs refers to the resistance of electrolyte out of porous part of an electrode. That is why the Rs increase is less than for Rf.

4. CONCLUSION

This work uses electrochemical impedance spectroscopy to estimate the parameters of a germanium phosphide electrode equivalent circuit at different charging-discharging cycles. It is concluded that prolonged cycling leads to an increase in the resistance of the solid electrolyte film, the charge transfer resistance, and the Warburg constant. The capacitance of the electric double layer and the resistance of the electrolyte change slightly during cycling. A change in the Warburg constant reflects the change of effective diffusion coefficient of sodium in germanium phosphide by order of magnitude.

CONFLICT OF INTERESTS
The authors declare no conflicts of interest.

References

1. K.-W. Tseng, S.-B. Huang, W.-C. Chang, and H.-Y. Tuan. *Chem. Mater*., 30 (2018) 4440.
2. H. Shen, Z. Ma, B. Yang, B. Guo, Y. Lyu, P. Wang, H. Yang, Q. Li, H. Wang, Z. Liu, and A. Nie. *J. Power Sources*, 433 (2019) Article No. 126682. https://doi.org/10.1016/j.jpowsour.2019.05.088.
3. X. Li, W. Li, P. Shen, L. Yang, Y. Li, Z. Shi, H. Zhang. *Ceram. Int.*, 45 (2019) 15711.
4. W. Li, X. Li, J. Liao, B. Zhao, L. Zhang, Y. Liu, L. Huang, Y. Li, M. Liu. *Energy Storage Materials,* 20 (2019) 380.
5. T. Zeng, H. He, H. Guan, R. Yuan, X. Liu, and C. Zhang. *Angew. Chem. Int. Ed*. 60 (2021) 12103.
6. W. Zhang, T. Liu, Y. Wang, Y. Liu, J. Nai, L. Zhang, O. Sheng, X. Tao. *Nano Energy*, 90 (2021) Article No. 106475.
7. T. Kulova, D. Gryzlov, A. Skundin, I. Gavrilin, Yu. Kudryashova, Nicolai Pokryshkin. *Int. J. Electrochem. Sci.*, 16 (2021) Article No. 211229.
8. A. Gasonoo, Y.-J. Lim, E.-J. Jang, Lee J., M.-H. Kim, Y. Choi, J.-H. Lee. *Mater. Today Energy*, 21 (2021) Article No. 100794. doi:10.1016/j.mtener.2021.100794.
9. S. Seki, Y. Kobayashi, H. Miyashiro, A. Yamanaka, Y. Mita, T. Iwahori. *J. Power Sources*, 146 (1-2) (2005) 741. doi:10.1016/j.jpowsour.2005.03.07.
10. C. N. Meddings, M. Heinrich, F. Overney, J.-S. Lee, V. Ruiz, E. Napolitano, S. Seitz, G. Hinds, R. Raccichini, M. Gaberšček, J. Park. *J. Power Sources*, 480 (2020) 228742. doi:10.1016/j.jpowsour.2020.228742.
11. Y.-M. Kang, J.-Y. Go, S.-M. Lee, W.-U. Choi. *Electrochem. Commun.*, 9(6) (2007) 1276.

doi:10.1016/j.elecom.2007.01.019.

12. R.-C. Lee, J. Franklin, C. Tian, D. Nordlund, M. Doeff, R. Kostecki *J. Power Sources*, 498 (2021) Article No. 229885. doi:10.1016/j.jpowsour.2021.22988.

13. J. Liu, J. Xu, Y. Chen, W. Sun, X. Zhou, J. Ke. *Int. J. Electrochem. Sci.*, 14 (2019) 359. doi: 10.20964/2019.01.08.

14. E.Yu. Evshchik, A.V. Korchun, A.V. Levchenko, Y.A. Dobrovolsky. *Int. J. Electrochem. Sci.*, 16 (2021) Article No. 151035, doi: 10.20964/2021.01.23.

15. T. K. Pham, J. H. Shin, N. C. Karima, Y. S. Jun, S.-K. Jeong, N. Cho, Y. Cho, S.N. Lim, W. Ahn. *J. Power Sources*, 506 (2021) Article No. 230244. doi:10.1016/j.jpowsour.2021.23024.

16. I.M. Gavrilin, V.A. Smolyaninov, A.A. Dronov, S.A. Gavrilov, A.Yu. Trifonov, T.L. Kulova, A.A. Kuz'mina, and A.M. Skundin. *Mendeleev Commun.*, 28 (2018) 659.

17. I.M. Gavrilin, Yu.O. Kudryashova, A.A. Kuz'mina, T.L. Kulova, A.M. Skundin, V.V. Emets, R.L. Volkov, A.A. Dronov, N.I. Borgardt, S.A. Gavrilov. *J. Electroanalyt. Chem.*, 888 (2021) Article No. 115209. https://doi.org/10.1016/j.jelechem.2021.115209.

18. W. Qi, H. Zhao, Y. Zeng, T. Tao, C. Chen, C. Kuang, S. Zhou, Y. Huang. *Sci. Rep.*, 7 (2017) 43582. https://doi.org/10.1038/srep43582.

19. H. Shen, Y. Huang, Y. Chang, R. Hao, Z. Ma, K. Wu, P. Du, B. Guo, Y. Lyu, P. Wang, H. Yang, Q. Li, H.T. Wang, Z. Liu, and A. Nie. *ACS Appl. Mater. Interfaces*,12 (2020) 17466.

20. N.-S. Choi, K.H. Yew, K.Y. Lee, M. Sung, H. Kim, S.S. Kim. *J. Power Sources*, 161 (2006) 1254.

21. C.C. Nguyen, S.W. Song. *Electrochim. Acta*, 55 (2010) 3026.

22. T.L. Kulova, A.A. Mironenko, A.M. Skundin, A.S. Rudy, V.V. Naumov, D.E. Pukhov. *Int. J. Electrochem. Sci.,* 11 (2016) 1370.